6. M. I. L'Vovich *et al.*, in *The Earth as Transformed by Human Action*, B. L. Turner *et al.*, Eds. (Cambridge Univ. Press, Cambridge, 1990), pp. 235–252.
7. P. M. Vitousek, P. R. Ehrlich, A. H. Ehrlich, P. A. Matson, *Bioscience* **36**, 368 (1986).
8. G. L. Ajtay, P. Ketner, P. Duvigneaud, in *The Global Carbon Cycle*, B. Bolin, E. T. Degens, S. Kempe, P. Ketner, Eds. (Wiley, New York, 1979), pp. 129–182.
9. Our global estimate conforms well to values derived from small-scale field studies with crops [B. A. Stewart, J. T. Musick, D. A. Dusek, *Agron. J.* **75**, 629 (1983); *Yield Response to Water* (U.N. Food and Agriculture Organization, Rome, 1979); Z. Zixi, B. A. Stewart, F. Xiangjun, *Field Crops Res.* **36**, 175 (1994)].
10. *1990 Production Yearbook* (U.N. Food and Agriculture Organization, Rome, 1991), with adjustments for United States and Taiwan based on data from U.S. Department of Agriculture.
11. E. Czaya, *Rivers of the World* (Van Nostrand Reinhold, New York, 1981).
12. Population estimates from C. Haub and M. Yanagishita, Population Reference Bureau (personal communication, Washington, DC, January 1995).
13. M. Dynesius and C. Nilsson, *Science* **266**, 753 (1994).
14. We do not include in our estimate of remote northern river flows a large number of rivers that have one or two dams (typically for hydropower) on their main channels but have flows vastly in excess of water supply needs in the region, including, for example, the Ob and Lena rivers of Siberian Russia, with a combined flow of 935 km^3. The ambitious Soviet scheme to divert water from the Ob to the Aral Sea basin would initially have involved 25 km^3/year, just 6% of the Ob's annual average flow. Likewise, a proposal to ship water via undersea pipeline from southeast Alaska to California involved 5 km^3 annually, just under 5% of the combined average annual flow of the Copper and Stikine rivers, leaving 95% of their flow still remote [*Alaskan Water for California? The Subsea Pipeline Option—Background Paper* (U.S. Office of Technology Assessment, Washington, DC, 1992)].
15. Uncaptured flood runoff provides a variety of human benefits, including support of flood-recession farming, fisheries, and generation of hydroelectricity; however, in these capacities, its use is either insignificant globally or does not involve actual appropriation.
16. Theoretically, a reservoir could be filled and emptied more than once a year, creating a greater effective capacity to regulate runoff than the storage capacity alone would indicate. We know of no estimates of this effective storage capacity other than the statement by K. Mahmood [*Reservoir Sedimentation: Impact, Extent, and Mitigation* (The World Bank, Washington, DC, 1987)] that the usable reservoir storage capacity "is nearly used once every year." We therefore make no adjustments to the estimated 3500 km^3 of capacity usable for runoff storage on an average annual basis.
17. This is a somewhat higher rate than is implied by Shiklomanov's estimates (*4*), which suggest rates of 10,700 to 11,000 m^3/ha. We arrived at our figure after examining data for California that suggest an average water application rate on that state's irrigated area of ~10,300 m^3 ha [*California Water Plan Update* (California Department of Water Resources, Sacramento, CA, 1994), vol. 1]. Because the average irrigation efficiency in California is reported to be 70%, which is substantially higher than the worldwide average [S. Postel, in (*5*), pp. 56–66], we believe that 12,000 m^3/ha is closer to the actual global average application rate. Moreover, the California figures account only for on-farm water applications and do not include the portion of diversions lost to seepage or evaporation between reservoirs and farmers' fields.
18. Evaporative losses from Lake Nassar, for example, have averaged 10 km^3/year, which is equal to 12% of the Nile's average annual flow [J. A. Allan, in *The Nile: Sharing A Scarce Resource*, P. P. Howell and J. A. Allan, Eds. (Cambridge Univ. Press, Cambridge, 1994), pp. 313–320].
19. H. E. Schwarz, J. Emel, W. J. Dickens, P. Rogers, J. Thompson, in *The Earth as Transformed by Human Action*, B. L. Turner *et al.*, Eds. (Cambridge Univ. Press, Cambridge, 1990), pp. 253–269.
20. Even in the countries of the Organization for Economic Cooperation and Development, domestic wastewater treatment is estimated to cover only ~60% of the population [A. K. Biswas, *Water Int.* **17**, 68 (February 1992)]. Information for developing countries is sparse, but treatment coverage is certainly far lower. Moreover, few regions control for farm runoff and other dispersed pollution sources that add substantial quantities of sediment, pesticides, and fertilizers to water bodies.
21. Even if wastewater treatment coverage should become nearly universal, substantial instream flows would still be required to maintain fisheries, support recreational demands, and satisfy other instream needs. For example, California's instream environmental water requirements (after omission of the north coast hydrologic region, which contains several wild and scenic rivers and thus may not be indicative of instream needs more narrowly defined) equal 22% of average annual runoff [*California Water Plan Update* (California Department of Water Resources, Sacramento, CA, 1994).
22. We did not consider it feasible to estimate accessible ET in a manner comparable to our estimate of AR. To be conservative, we therefore assumed all terrestrial ET to be accessible.
23. Wangnick Consulting, *1990 IDA Worldwide Desalting Plants Inventory* (International Desalination Association, Englewood, NJ, 1990).
24. P. H. Gleick, *Annu. Rev. Energy Environ.* **19**, 267 (1994).
25. J. A. Veltrop, in *Water for Sustainable Development in the Twenty-first Century*, A. K. Biswas, M. Jellali, G. E. Stout, Eds. (Oxford Univ. Press, Oxford, 1992), pp. 102–115.
26. *Status of Dam Construction, 1991* (International Commission on Large Dams, Paris, 1992), suggests that ~300 dams are now commissioned each year, but these data include only 64 countries.
27. A. P. Covich [in (*5*), pp. 40–55] indicates that large dams are currently being completed at an average rate of 500 per year, or 56% of the rate of the period from 1950 to 1986.
28. Because ~85% of existing large dams were built since mid-century (*25*), this calculation assumes that 85% of total existing storage capacity was constructed since then, or 4675 km^3 (5500 km^3 × 0.85). With the assumption that 40% as many dams would be constructed between 1990 and 2025 as between 1950 and 1985, and that capacity per dam remains constant, 1870 km^3 (4675 km^3 × 0.40) of capacity would be added by ca. 2025, of which 1190 km^3 would be live storage for water supply.
29. Even as dam construction is adding to the total stable runoff, other human activities are reducing it. Deforestation and the paving over of aquifer recharge areas often reduce rainwater infiltration, thereby reducing base flow and increasing surface flood runoff. More important globally, many reservoirs are losing active storage capacity faster than originally estimated because of rapid siltation from deforestation, soil erosion, and generally poor watershed management. The Nizamsagar reservoir in India, for instance, lost more than 60% of its capacity over 40 years [M. Newson, *Land, Water and Development: River Basin Systems and Their Sustainable Management* (Routledge, London, 1992]. Lacking global estimates, we make no subtraction for these losses.
30. P. E. Waggoner, Ed., *Climate Change and U.S. Water Resources* (Wiley, New York, 1990).
31. National Research Council, *Restoration of Aquatic Ecosystems* (National Academy Press, Washington, DC, 1992).
32. *1994 World Population Data Sheet* (Population Reference Bureau, Washington, DC, 1994).
33. We gratefully acknowledge comments from W. Falcon, P. Gleick, R. Naylor, A. Vickers, P. Vitousek, and two anonymous reviewers. Supported by a grant from Charles and Nancy Munger, the Winslow and Heinz foundations, and an anonymous donor.

28 September 1995; accepted 21 December 1995

Rapid Collapse of Northern Larsen Ice Shelf, Antarctica

Helmut Rott, Pedro Skvarca, Thomas Nagler

In January 1995, 4200 square kilometers of the northern Larsen Ice Shelf, Antarctic Peninsula, broke away. Radar images from the ERS-1 satellite, complemented by field observations, showed that the two northernmost sections of the ice shelf fractured and disintegrated almost completely within a few days. This breakup followed a period of steady retreat that coincided with a regional trend of atmospheric warming. The observations imply that after an ice shelf retreats beyond a critical limit, it may collapse rapidly as a result of perturbated mass balance.

Ice shelves cover 11% of the total area of Antarctica (*1*) and play an important role in the mass budget and dynamics of the Antarctic Ice Sheet. Most of the ice that has accumulated over the grounded parts of Antarctica is discharged to ice shelves, where it is lost as icebergs along the seaward edges as well as by basal melting (*2*). Because ice shelves are exposed to both atmosphere and ocean, they are sensitive to changes in the temperature and circulation of either (*3*). The 0°C summer isotherm has been taken as the climatic limit for the existence of ice shelves along the west coast of the Antarctic Peninsula (*4*). Between 1966 and 1989, the Wordie Ice Shelf (Fig. 1) decreased from ~2000 to 700 km^2, probably as a result of regional atmospheric warming (*5*). Here, we report on the recent disintegration of the northern Larsen Ice Shelf (LIS).

The LIS extends along the eastern side of the Antarctic Peninsula from latitude 64° to 74°S (Fig. 1). The part of the LIS north of Robertson Island has retreated slowly but constantly since the 1940s (*6, 7*). The retreat accelerated after 1975 (*8*), and

H. Rott and T. Nagler, Institut für Meteorologie und Geophysik der Universität Innsbruck, Innrain 52, A-6020 Innsbruck, Austria.
P. Skvarca, Instituto Antártico Argentino, Cerrito 1248, 1010 Buenos Aires, Argentina.

finally two parts of the ice shelf collapsed early in 1995. We analyzed this collapse with the use of sequences of synthetic aperture radar (SAR) images from the ERS-1 satellite (9). The satellite data analysis was complemented by field observations made during October and November 1994.

For the analysis, we separated the ice shelf north of Jason Peninsula (Fig. 2) into four sections: section 1, Jason Peninsula to Seal Nunataks; section 2, the area around Seal Nunataks; section 3, Seal Nunataks to Sobral Peninsula; and section 4, the remnant part between James Ross Island and the Antarctic Peninsula (*10*). Sections 1, 3, and 4 receive major ice input from grounded zones (*11*). The ratios of grounded catchment basin to floating ice shelf area in sections 1, 3, and 4, based on the ice shelf extent in March 1986 (Table 1), were clearly smaller than the ratios for most other Antarctic ice shelves. However, because the accumulation on the glaciers descending from the peninsula plateau is up to four times the accumulation on the ice shelf (*12*), it can be concluded that the ice contributed by grounded parts surpassed the mass accumulated in situ. Section 2 is an almost stagnant part of the ice shelf that is cut off from the ocean by ice-covered Robertson Island and separates the faster flowing sections to the north and south. The ice shelf in Larsen Inlet (Fig. 2) disappeared almost completely between March 1986 and November 1989 (8).

The ice front between Jason Peninsula and Robertson Island (section 1) showed a comparatively constant seaward advance between 1975 and 1992. The total displacement was 5 to 6 km, with little calving loss (6). The main part of the ice front advanced until 25 January 1995, but small icebergs broke away from the heavily rifted zone south of Robertson Island after July 1992. A major rift of ~25 km in length, corresponding to the later calving front south of Robertson Island, was already visible in the SAR image of July 1992 and looks similar in the image of 25 January 1995. A large iceberg covering 1720 km^2, and many small pieces corresponding to a previous ice shelf area of 550 km^2, broke away between 25 and 30 January 1995 (Fig. 2). Although major calving losses after extended periods of ice front advance are characteristic of ice shelves, the temporal coincidence of this calving with the disintegration events farther north may indicate the beginning of a period of major retreat.

The most rapid retreat was observed for the part of the ice shelf between Seal Nunataks and Sobral Peninsula (section 3). The two main tributaries to this section are Drygalski Glacier and the Dinsmoor, Bombardier, and Edgeworth (D-B-E) glaciers, which form a single stream at the grounding line. The SAR image of 16 February 1993 shows that the ice surface was covered by a

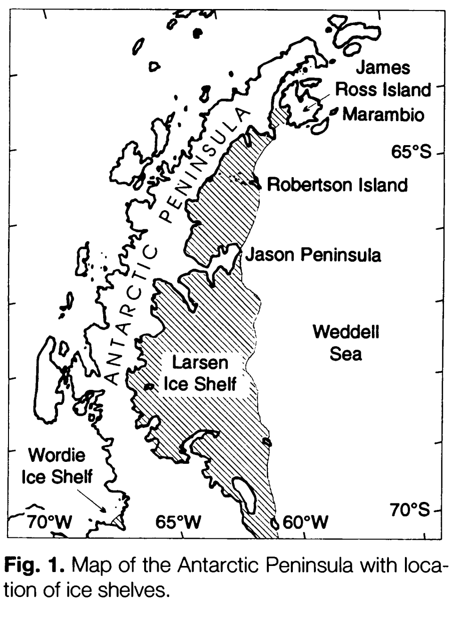

Fig. 1. Map of the Antarctic Peninsula with location of ice shelves.

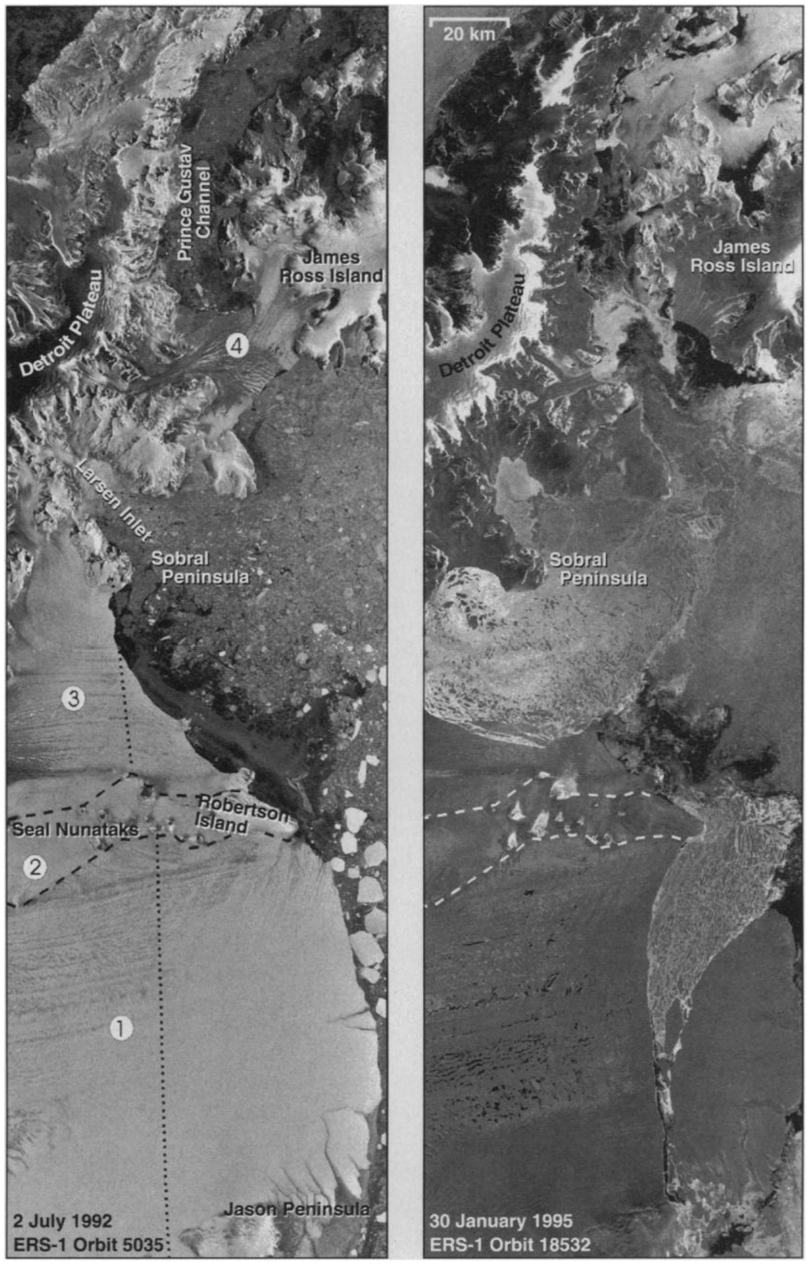

Fig. 2. Mosaic of ERS-1 SAR images (*10*) of the northern LIS from 2 July 1992 (left) and 30 January 1995 (right). Section numbers are circled; dashed lines indicate separations between sections 1, 2, and 3. Dotted lines are profiles of field measurements. The image brightness is related to the intensity of the backscattered radar signal. In the July image, the snow and ice surfaces appear bright because the frozen firn and ice produce high radar backscatter, whereas the backscatter from the melting surfaces in January is low (*26*).

pattern of undulating melt streams and lakes aligned in the direction of the ice flow (Fig. 3). From 1975 to 1989, the ice front between Lindenberg Island and Sobral Peninsula retreated at an average rate of ~1 km/year (*8*). The retreat accelerated during summer 1992–1993, when 209 km^2 of the ice shelf were lost within 10 weeks, compared with 241 km^2 during the previous 6.5 years.

The retreat slowed between February 1993 and November 1994, but the fracturing process intensified. Until October–November 1991, the ice shelf (with the exception of the area downstream of the D-B-E glaciers) was almost ideally flat, with no distinct rifts and few crevasses. Field observations in late 1994 showed that the surface morphology was quite different. The main parts of the ice shelf contained gentle large-scale surface undulations, and several rifts many kilometers in length had formed approximately parallel to the ice front. The rifts separated plates that differed by as much as several meters in surface height, which implied that the fractures cut completely through the ice. Downstream of the D-B-E glaciers, the ice was heavily crevassed; at one location, an ice wedge rose 15 m above the level ice shelf. Although major parts of the ice shelf were already strongly fractured, a combination of cold temperatures and a dense cover of fast ice extending many kilometers seaward evidently kept the ice shelf from breaking apart.

The final disintegration of section 3 started during a period of intense northwesterly winds and high temperatures after 20 January 1995. Between November 1994 and 25 January 1995, the ice front between Lindenberg Island and Sobral Peninsula retreated by 3 km on average, followed by a further retreat of ~2 km between 25 and 28 January. During the next 2 days, the disintegration process accelerated considerably (Fig. 4). By 30 January, parts of the ice boundary north of Drygalski Glacier had already retreated to the grounding line. The ice broke into comparatively small pieces. The maximum distance covered by an iceberg within 56.5 hours was 42 km (Fig. 4). The forces acting on icebergs driven by the wind (*13*) caused the icebergs to drift at 40° to 90° to the left of the estimated surface wind direction. The rotation and convergence of the icebergs during these 2 days indicated an additional influence from ocean currents.

On 2 February, the ice along the northern and eastern boundary of Larsen Nunatak broke away, shifting the seashore close to Matienzo station on this nunatak (*14*). The ice front between Robertson and Lindenberg islands remained stable; oblique aerial photography from 3 March 1995 showed that a small strip of the ice shelf still linked the two islands. Between November 1994 and March 1995, the area of section 3 decreased from 1960 to 320 km^2 (*15*).

The ice shelf across Prince Gustav Channel (section 4) was separated from the main part of the LIS sometime in 1957 or 1958 (*7*). It was nourished by ice drainage from the Antarctic Peninsula (with Sjögren and Boydell glaciers as the main tributaries), by ice input from James Ross Island, and by long-term snow accumulation on fast sea ice (Fig. 5). The ice from Sjögren and Boydell glaciers extended eastward toward Persson Island, whereas ice from James Ross Island touched the eastern side of Persson Island and extended several kilometers farther westward to the south of the island. The position of the northern ice front did not change much between 1957 and 1986 (*6*); the only major change occurred at the coast of Cape Obelisk, where a polynya is visible in the Landsat image of 1 March 1986. The southern ice front retreated by ~15 km between 1958 and 1969 (*7*), was almost stationary between 1969 and 1986, and showed further retreat by ~5 km between 1986 and August 1993.

The final disintegration of section 4 started in the north with the detachment of the ice boundary along the coast near Cape Obelisk, which eliminated constraining backforces for the ice downstream from Sjögren and Boydell glaciers. In response to changes of the strain field in this area, the ice front advanced as much as 350 m from February 1988 to November 1989. The main part of this ice broke away during summer 1992–1993 (*16*). On 30 January 1995, two small parts of the ice shelf re-

Table 1. Ratios of grounded catchment basin to floating ice shelf area (A_g/A_f) on 1 March 1986, and ice shelf areas from Landsat images (1 March 1986) and from ERS-1 SAR images (other dates).

Location	A_g/A_f (1 March 86)	Area (km^2)			
		1 March 86	2 July 92	26 August 93	30 January 95
Section 1	0.74	11,560	11,775	11,770	9,496
Section 3	1.07	2,488	2,244	2,027	1,101*
Section 4	1.66	984	762	528	224
Larsen Inlet	1.94	399	36	26	24

*The area of section 3 further decreased to 320 km^2 after 30 January 1995.

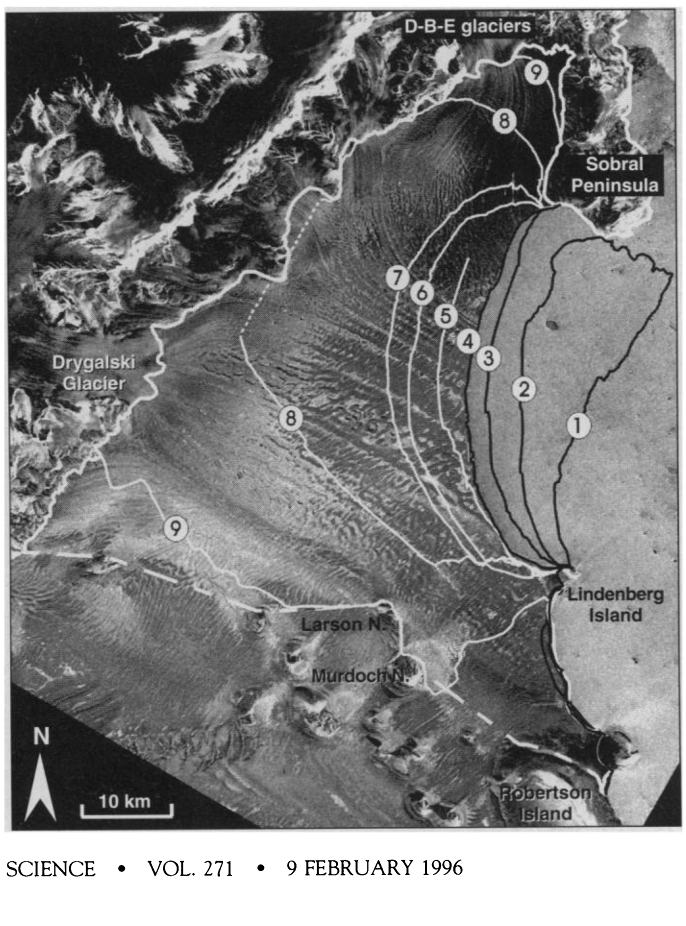

Fig. 3. ERS-1 SAR image of the LIS north of Seal Nunataks, acquired on 16 February 1993, with ice front positions (circled numbers) superimposed as follows: 1, 1 March 1986; 2, 8 December 1992; 3, 12 January 1993; 4, 16 February 1993; 5, 23 October 1994; 6, 25 January 1995; 7, 28 January 1995; 8, 30 January 1995; and 9, 22 March 1995. Bold white line, grounding line; dashed line, boundary between sections 2 and 3 (see Fig. 2). Data for the ice front positions are from ERS-1, except for positions 1 (Landsat), 5 (field observations), and 9 (NOAA).

mained on the west coast, and another part remained in Röhss Bay. A National Oceanic and Atmospheric Administration (NOAA) image from 9 January 1995 shows that although the channel was open, major icebergs were close to the previous ice shelf, which indicated that the shelf had broken only a few days earlier.

An ice shelf is thought to be able to survive small temporary perturbations of the mass balance, but not large prolonged ones (*17*). Changes in the total mass of an ice shelf are determined by the mass added or removed at the surface and on the bottom, by the rate of ice supply from grounded areas, and by the amount of ice exported in calving. Mass balance data are available for the period 1980 to 1994 along the profile in section 1, for the period 1978 to 1994 for five points of section 2, and for the period 1984 to 1994 for two points of section 3. The specific mass balance (*18*) decreased from 180 mm/year close to Jason Peninsula in the south to 70 mm/year for the ice shelf north of Larsen Nunatak. Taking into account the estimated total snow accumulation of 200 to 250 mm/year, this decrease indicates an increasing loss of meltwater to the sea to the north. No information is available on basal melting or freezing. The stagnant ice of section 2 suggests that, at least for this part of the ice shelf, basal melting and surface mass balance have been approximately equal in the long term. However, the retreat of the ice front likely resulted in increased basal melt rates in some parts of sections 3 and 4, because the melt rates are usually highest close to the ice front (*3*).

Increased surface melt in recent summers, and possibly also increased basal melt, were certainly important factors in the accelerated retreat. At five points west of Seal Nunataks, the surface mass balance was close to zero for the period November 1988 to October 1994, whereas between 1978 and 1988 it was 200 mm/year. Similar long-term changes in annual mass balance were observed along the profile in section 1 (*19*). Fast retreat and final disintegration of the northernmost sections of the LIS took place during a period of warm summers, which began during 1986–1987 and included the two warmest summers recorded at Marambio station (Fig. 1): The mean temperatures were +0.2°C during summer 1992–1993 and +0.6°C during summer 1994–1995, compared to a mean of –2.0°C for the 24-year record. Mean annual air temperatures for stations at the Antarctic Peninsula have increased since the 1950s (*20*). The longest climatological record in this region (since 1904 at Orcadas station, South Orkney Island) indicates that this warming trend extends back to the 1930s (*21*). The retreat of the northern LIS, in accordance with the retreat of the ice shelves at the west coast of the Antarctic Peninsula (*5*) and of the tidewater glaciers of James Ross Island (*22*), is another indicator of changes in regional climate.

The rapidity of the collapse further implicates the dominant role of fracture dynamics in ice shelf disintegration (*17*). The closest time sequence of the event is available for section 3. As long as the ice front was normal to the flow lines, transverse rifting was the primary mechanism for iceberg calving. The retreat of the ice front along Sobral Peninsula resulted in a decrease of lateral drag in the northern part, whereas in the south, Lindenberg Island acted as a pinning point that maintained the ice front south of the island (Fig. 3). Consequently, the resulting stress vector at the ice front north of Lindenberg Island rotated counterclockwise until it was finally aligned approximately parallel to the flow lines, triggering longitudinal rifting in addition to transverse rifting (*23*). Fractures related to tidal motion along the grounding line were also important, as were fractures related to motion discontinuities along the boundary of sections 2 and 3 (where we observed upwelling water even during cold periods). Another critical zone was the area downstream of the D-B-E glaciers where the ice flow changed direction by 90° and diverged laterally (*24*). During summer, infiltration of meltwater from the surface and upwelling of seawater accelerated the fracturing. Other triggers for the final disintegration were likely the presence of strong winds, predominantly from the northwest, and high air temperatures during the last 10 days of January. During the peak period, 23 to 26 January, the mean wind velocity at Marambio station was 49 knots (*25*). After the ice had retreated gradually beyond a certain critical limit, these factors finally caused the complete disintegration of the ice shelves within a few days.

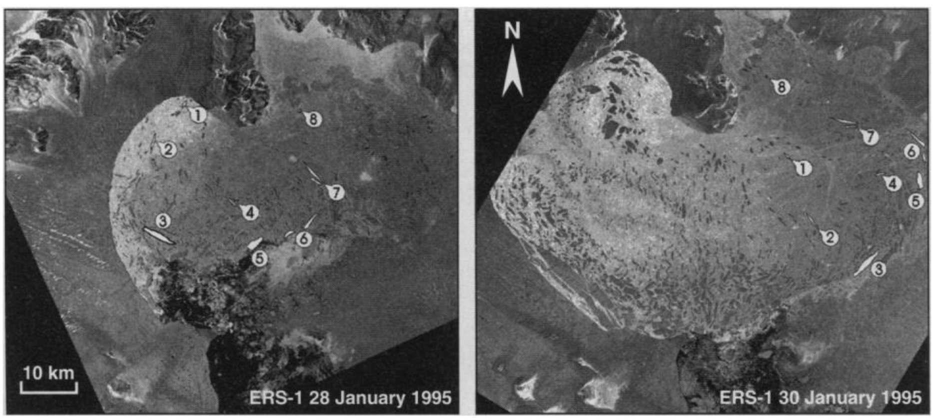

Fig. 4. ERS-1 SAR images acquired on 28 January 1995, 04:08 GMT (left), and 30 January 1995, 12:46 GMT (right). Several icebergs are enhanced and numbered to illustrate the drift.

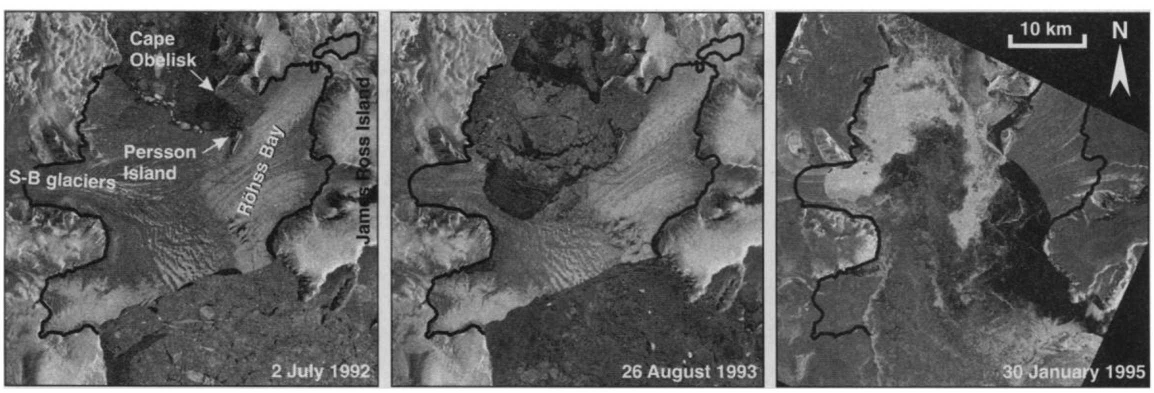

Fig. 5. ERS-1 SAR images acquired on 2 July 1992, 26 August 1993, and 30 January 1995, showing the ice shelf between the Antarctic Peninsula and James Ross Island. The grounding line is shown in black; S-B, Sjögren-Boydell glaciers.

Our observations suggest that ice shelves close to the climatic limit for existence may disintegrate rapidly. During the next years, increased attention should be paid to the section of the LIS south of Seal Nunataks, which may be subject to major changes if the warming continues. In November 1994, we observed a transverse rift ~50 km in length in section 1, ~30 km inland from the ice front.

REFERENCES AND NOTES

1. C. Swithinbank, *U.S. Geol. Surv. Prof. Pap. 1386-B* (1988).
2. S. S. Jacobs, H. H. Helmer, C. S. M. Doake, A. Jenkins, R. M. Frolich, *J. Glaciol.* **38**, 375 (1992).
3. A. Jenkins and C. S. M. Doake, *J. Geophys. Res.* **96**, 791 (1991).
4. J. H. Mercer, *Nature* **271**, 321 (1978).
5. C. S. M. Doake and D. G. Vaughan, *ibid.* **350**, 328 (1991).
6. P. Skvarca, *Ann. Glaciol.* **20**, 6 (1994).
7. C. S. M. Doake, *ibid.* **3**, 77 (1982).
8. P. Skvarca, *ibid.* **17**, 317 (1993).
9. The ERS-1 SAR images were acquired at the German receiving station near the Chilean Antarctic Base O'Higgins, operating on a campaign basis. The northern LIS was imaged by ERS-1 SAR in July 1992, between December 1992 and February 1993, in August 1993, and between mid-January and mid-February 1995. For comparison with conditions previous to the accelerated retreat, we analyzed Landsat Multispectral Scanner (MSS) images from 1 March 1986.
10. We obtained the ERS-1 SAR data in Universal Transverse Mercator projection based on the WGS-84 ellipsoid with nominal spatial resolution of 25 m by 25 m and location accuracy of better than 100 m in areas of low relief. We used geodetic field data to control and improve the absolute location accuracy. Geometric accuracy was high only close to sea level, because terrain-induced distortions resulting from radar imaging geometry could not be corrected because of a lack of high-resolution elevation data.
11. Data on ice motion, surface mass balance, and ice thickness were obtained for sections 1, 2, and 3 during field observations beginning in the early 1980s. Mean annual velocities from 1984 to 1994 in the center of the profiles (Fig. 2) were 385 m/year in section 1 and 248 m/year in section 3. Ice thicknesses at the same points were 250 m (section 1) and 220 m (section 3).
12. D. A. Peel, in *The Contribution of the Antarctic Peninsula to Sea Level Rise*, E. M. Morris, Ed. (British Antarctic Survey, Cambridge, 1992), pp. 11–15.
13. W. M. Sackinger, M. O. Jeffries, H. Tippens, F. Li, M. Lu, *Ann. Glaciol.* **12**, 152 (1989).
14. N. Contreras, unpublished data.
15. The value of 320 km^2 was derived from an image of the Advanced Very High Resolution Radiometer (AVHRR) of the NOAA satellite with 1-km spatial resolution, acquired on 22 March 1995. An ERS-1 image from 11 February 1995, covering the area around Seal Nunataks, shows the southern ice boundary close to the position of 22 March.
16. Because of a lack of images, the exact date of the final opening of Prince Gustav Channel is not known.
17. T. Hughes, *J. Glaciol.* **29**, 98 (1983).
18. Surface mass balance was determined from measurements at stakes and snow pits. The specific mass balance is the change of mass per unit area within a given time period (the algebraic sum of accumulation and ablation). Mass balance for an entire glacier or ice shelf represents the overall change in mass.
19. The specific mass balance averaged over sites 15, 25, and 35 km south of Seal Nunataks revealed the following temporal changes: 1980 to 1988, 220 mm/year; 1988 to 1991, 130 mm/year; and 1991 to 1994, −70 mm/year.
20. J. C. King, *Int. J. Climatol.* **14**, 357 (1994).
21. J. A. J. Hofmann, in *Actas, Primera Conferencia Latinoamericana sobre Geofísica, Geodesia e Investigación Espacial Antárticas,* Buenos Aires, 30 July to 3 August 1990, p. 160 (1991).
22. P. Skvarca, H. Rott, T. Nagler, *Ann. Glaciol.* **21**, 291 (1995).
23. The following conditions for stability [J. Oerlemans and C. J. van der Veen, *Ice Sheets and Climate* (Reidel, Dordrecht, Netherlands, 1984), pp. 41–64] were no longer valid after the retreat of the LIS along Sobral Peninsula: (i) The gradient thickness H along a flow line in direction x for a stable ice shelf in an embayment with two parallel sides is given by

$$\frac{\partial H}{\partial x} = \frac{\tau_s}{\rho_i g[1 - (\rho_i/\rho_w)]W}$$

where τ_s is the shear stress at the sidewalls, g is the acceleration of gravity, ρ_i and ρ_w are the density of ice and water, respectively, and W is the width of the ice shelf. When the ice front retreated into the bay west of Sobral Peninsula, W became enlarged suddenly, violating the stability criterion. (ii) The shear strain ($\partial u/\partial y + \partial v/\partial x$) at a stable ice front is zero, where u is the velocity in direction x of the flow line and v is the velocity in direction y. This essentially means that the front is perpendicular to the flow lines. After 1986, the ice front north of Lindenberg Island differed increasingly from this stable geometry.
24. R. A. Bindschadler, M. A. Fahnestock, P. Skvarca, T. A. Scambos, *Ann. Glaciol.* **20**, 319 (1994).
25. A wind velocity of 49 knots results in a surface stress due to wind shear of ~1 N m^{-2}. For an undisturbed ice shelf of the size of the LIS, this force would be ~0.1 to 0.2% of the stress due to shear at the sidewalls. For the breakup of a heavily disturbed ice shelf, even these small forces due to wind may play a role, as may the effects of wind on ocean circulation. An increased probability of calving events during periods of persistent offshore winds and air temperatures above 0°C has been reported for Arctic ice shelves [M. O. Jeffries, *Rev. Geophys.* **30**, 245 (1992)].
26. H. Rott, K. Sturm, H. Miller, *Ann. Glaciol.* **17**, 337 (1993); H. Rott and C. Mätzler, *ibid.* **9**, 195 (1987).

27. The ERS-1 SAR data (from ERS-1 Experiment AO1.A2 and ERS-1/ERS-2 Experiment AO2.A101) were provided by the European Space Agency. The temperature data from Marambio station were provided by Servicio Meteorológico Nacional, Fuerza Aérea Argentina. This work is a contribution to Austrian Science Fund (FWF) Project 10709-GEO, to the National Space Research Program of the Austrian Academy of Sciences, and to the Larsen Ice Shelf Project of Instituto Antártico Argentino, Direcciòn Nacional del Antártico.

5 September 1995; accepted 14 November 1995

DNA: An Extensible Molecule

Philippe Cluzel, Anne Lebrun, Christoph Heller,* Richard Lavery, Jean-Louis Viovy, Didier Chatenay,† François Caron‡

The force-displacement response of a single duplex DNA molecule was measured. The force saturates at a plateau around 70 piconewtons, which ends when the DNA has been stretched about 1.7 times its contour length. This behavior reveals a highly cooperative transition to a state here termed S-DNA. Addition of an intercalator suppresses this transition. Molecular modeling of the process also yields a force plateau and suggests a structure for the extended form. These results may shed light on biological processes involving DNA extension and open the route for mechanical studies on individual molecules in a previously unexplored range.

Many biologically important processes involving DNA are accompanied by deformations of the double helix, and the ability of DNA to stretch "like a spiral spring in tension" (*1*, p. 739) was recognized long ago (*1–3*). The mechanics of DNA has regained interest in recent years as a result of the possibility of working with individual molecules. The extension of a duplex DNA molecule under the action of an external force was measured by Smith *et al.* (*4*) and compared to predictions of the wormlike chain model (*5*). In good agreement with this theory, these researchers observed that a force of 2 to 3 pN is able to stretch the DNA to 90% of its contour length at rest in the B-form, l_0, and that the force then rises sharply when the extension approaches l_0. This experiment was restricted to forces smaller than 20 to 30 pN, whereas it has been suggested that DNA is able to withstand about 500 pN before breaking (*6*). We present here a study of the force-extension response of a single duplex DNA molecule submitted to forces ranging from 10 to 160 pN, using an apparatus (Fig. 1) that improves on that developed by Kishino and Yanagida to study the actin-myosin interaction (*7*).

We repeated our experiment many times using different fibers and stretching velocities (a few seconds was typically required for stretching). Two types of curves were ob-

P. Cluzel, C. Heller, J.-L. Viovy, Institut Curie [URA Centre National de la Recherche Scientifique (CNRS) 448 and 1379], 11–13 Rue Pierre et Marie Curie, Paris 75005, France.

A. Lebrun and R. Lavery, Laboratoire de Biochimie Théorique (URA77 CNRS), Institut de Biologie Physico-Chimique, 13 Rue Pierre et Marie Curie, Paris 75005, France.

D. Chatenay, LUDFC, Institut de Physique, 3 Rue de l'Université, Strasbourg 67084, France.

F. Caron, Ecole Normale Superieure, Laboratoire de Génétique Moléculaire (URA CNRS 1302), 46 Rue d'Ulm, Paris 75230, France.

*Permanent address: Max-Planck-Institut für Molekulare Genetik, Ihnestraße 73, D-14195 Berlin-Dahlem, Germany.

†Present address: Rockefeller University, Box 265, 1230 York Avenue, New York, NY 10021, USA.

‡To whom correspondence should be addressed.